Research Square

Preprints are preliminary reports that have not undergone peer review.
They should not be considered conclusive, used to inform clinical practice,
or referenced by the media as validated information.

Transcriptome-wide assessment of the m^{6}A methylome of intestinal porcine epithelial cells treated with deoxynivalenol

Zhengchang Wu
Yangzhou University
Chao Xu
Yangzhou University
Haifei Wang
Yangzhou University
Song Gao
Yangzhou University
Shenglong Wu
Yangzhou University
Wenbin Bao (wbbao@yzu.edu.cn)
Yangzhou University https://orcid.org/0000-0001-5486-2253

Research

Keywords: N6-methyladenosine, IPEC-J2, Deoxynivalenol, Transcriptome

Posted Date: September 16th, 2020

DOI: https://doi.org/10.21203/rs.3.rs-73169/v1

License: This work is licensed under a Creative Commons Attribution 4.0 International License. Read Full License

Abstract

Background: Deoxynivalenol (DON) is a cytotoxic compound found in various food and feed products. N^6-Methyladenosine (m^6A) is a highly abundant epitranscriptomic marker that modifies a wide range of mRNA molecules in mammalian cells. However, the role of the m^6A methylome in DON-induced damage remains poorly understood.

Results: In this study, we assessed the transcriptome-wide m^6A profile of intestinal porcine epithelial cells (IPEC-J2) treated with 1000 ng/mL DON by m^6A sequencing and RNA sequencing. Overall, 5406 new m^6A peaks appeared with the disappearance of 2615 peaks in DON-treated IPEC-J2 cells. Genes that were uniquely m^6A-modified following DON treatment were found to be associated with the tumor necrosis factor (TNF) signaling pathway. On comparing DON-treated and control cells, we identified 733 differentially expressed mRNAs bearing hyper- or hypomethylated m^6A peaks. Further experimental data suggested that METTL3-dependent m^6A methylation might also play a role in DON-induced inflammatory response, and *CSF2* marker is key functional relevance in the context of DON-induced toxicity.

Conclusions: This is the first study to perform a transcriptome-wide assessment of the m^6A methylome of IPEC-J2 cells treated with DON. We believe that our findings should be useful for identifying mechanisms whereby m^6A modifications influence the outcomes of DON exposure.

Background

RNA modifications can modulate the stability, function, and metabolic processing of modified RNAs. To date, five primary types of RNA methylation have been described: 5-methylcytosine (m^5C), N^7-methylguanine (m^7G at the 5'-cap), N^6-methyladenosine (m^6A), N^1-methyl adenosine (m^1A), and pseudouridine (ψ) [1]. Among these, m^6A modifications are the most common and functionally important internal RNA modifications within eukaryotic cells, wherein they serve as key regulators of gene expression [2]. In general, the distribution of m^6A modifications is most commonly associated with the stop codon (stopC), transcriptional start site (TSS) sequences, coding sequence (CDS), 3'-untranslated region (3'-UTR) sequences, and 5'-UTR sequences in modified RNAs [3]. These m^6A modifications can profoundly impact RNA splicing, nuclear export, translation, and degradation [4]. As such, they are closely linked to normal physiological processes, including gametogenesis and cell division, and to pathological conditions, such as cancer and infertility [5]. There is also evidence that m^6A modifications are involved in viral replication [6] and the modulation of host–pathogen interactions [7, 8]. While many studies on m^6A modifications have been conducted in humans and mice, few have assessed the relationship among these modifications and vital traits in poultry and livestock. Analyses of m^6A methylation in pigs have largely focused on the impact of these modifications on fat deposition [9], lipid metabolism [10], stem cell differentiation [11], and liver development [12]. No comprehensive studies have as yet characterized the transcriptome-wide distribution of m^6A modifications in the context of most porcine diseases, underscoring a novel direction for the ongoing epigenetic studies on economically important livestock.

Mycotoxins are secondary metabolites derived from fungi that often contaminate human and animal food supplies and induce significant cytotoxic damage following consumption [13]. Deoxynivalenol (DON) is among the most important mycotoxins associated with impaired intestinal integrity; moreover, it evidently exhibits proinflammatory and immunomodulatory properties [14]. In some previous studies involving an intestinal porcine epithelial cell line (IPEC-J2), exposure to DON was found to induce oxidative stress and inflammation, eventually causing accelerated apoptotic cell death and impaired functionality [15–18]. The m^6A status of DON-treated IPEC-J2 cells has not been assessed so far. Thus, we herein conducted an m^6A-specific RNA immunoprecipitation assay using the methylated RNA immunoprecipitation sequencing (MeRIP-seq) approach [19] to examine the transcriptome-wide m^6A modification profile of control and DON-treated cells. Accordingly, we identified distinct m^6A modification patterns associated with DON treatment; we further used bioinformatics and qPCR to identify key signaling pathways and genes related to dysregulated m^6A methylation in IPEC-J2 cells. We believe that our findings should serve as a foundation for future studies on the roles of m^6A modification in the context of DON-induced cell damage.

Methods

Cell Culture

IPEC-J2 cells were obtained from the University of Pennsylvania (PA, USA) and cultured in DMEM/F12 containing 10% fetal bovine serum at 37°C in a 5% CO_2 incubator. For viability analyses, the cells were added to 96-well plates (2×10^4/well) for 12 h, and then treated with 1000 ng/mL DON (Sigma, Germany) for 24, 48, or 72 h. The Cell Counting Kit-8 (Dojindo, Japan) assay was performed to examine cell viability, as per manufacturer instructions. To assess apoptosis, the cells were treated with DON (1000 ng/mL) for 48 h, followed by staining using the Annexin V-FITC/PI Apoptosis Detection Kit (Solarbio, Beijing, China). For RNA-based experiments, IPEC-J2 cells were added to 6-well plates (1×10^6/well) and incubated until 80% confluence; the cells were subsequently treated with DON (1000 ng/mL) for 48 h. They were then collected for downstream analyses.

m^6A MeRIP-seq and RNA-seq

For RNA-seq, three pairs of control and DON-treated cell samples were harvested. TRIzol (Invitrogen, CA, USA) was used for total RNA extraction, and RNA quality was assessed using a NanoDrop ND-1000 spectrophotometer (Thermo Fisher Scientific, MA, USA). MeRIP-seq and RNA-seq were performed by CloudSeq Biotech Inc. (Shanghai, China) using previously reported methods [19]. Briefly, the GenSeq™ m^6A-MeRIP Kit (GenSeq Inc., China) was used, as per manufacturer instructions, to conduct m^6A RNA immunoprecipitation. The immunoprecipitated (IP) and control input samples were then used for RNA-seq library preparation with the NEBNext® Ultra II Directional RNA Library Prep Kit (New England Biolabs, Inc., USA). An Agilent 2100 Bioanalyzer (Agilent Technologies, Inc., USA) was used to confirm the quality of the prepared libraries, and an Illumina HiSeq 4000 sequencer (Illumina, Inc.) was used for library sequencing with 150 bp paired-end reads. The raw high-throughput m^6A and RNA-seq data have been uploaded to the Gene Expression Omnibus database (accession no.: GSE156078).

Sequencing data analysis

After sequencing, the samples were subjected to Q30-based quality control. Following 3'-adaptor-trimming, low-quality reads were removed using Cutadapt v1.9.3 [20]. Clean library reads were aligned to a reference genome (Sscrofa11.1, https://www.ncbi.nlm.nih.gov/genome/?term=pig) with Hisat2 v2.0.4 [21]. MACS2 v.2.1.2 was then used to identify m^6A peaks in MeRIP-seq data [22]. m^6A peaks that overlapped with transcript exons were selected for further evaluation. Differences in m^6A methylation rates between DON-treated and control cells were compared using diffReps [23]. Peaks that were significantly different between the groups met the following criteria: $\log2|\text{fold change}| \geq 1$ and FDR ≤ 0.05. These peaks were then subjected to gene ontology (GO) and Kyoto Encyclopedia of Genes and Genomes (KEGG) pathway enrichment analyses.

The m^6A peak distribution patterns associated with different functional regions (TSS, CDS, stopC, 3'-UTR, 5'-UTR) were assessed, and m^6A peaks along the entire transcript were assessed using the Integrative Genomics Viewer tool [24]. Significant motifs among these peak sequences were detected using MEME suite (http://meme-suite.org/) and DREME (http://memesuite.org/tools/dreme). The HTSeq program (v0.9.1) was used to obtain raw mRNA-seq read data, which were normalized using edgeR. GO (www.geneontology.org) and KEGG pathway (www.genome.jp/kegg) enrichment analyses of differentially expressed mRNAs and differentially methylated genes were then performed.

qPCR analysis

TRIzol (Invitrogen) was used for total RNA isolation from IPEC-J2 cells, as stated earlier, and cDNA was obtained using the PrimeScript RT-PCR Kit (TaKaRa, Beijing, China). qPCR was performed on an ABI7500 instrument (Applied Biosystems, CA, USA) with the following thermocycler settings: 95°C for 30 s, followed by 40 cycles of 95°C for 5 s and 60°C for 34 s. The expression levels of the following genes were assessed: *CSF2*, *KLF6*, *CCR7*, *CCL5*, *KLF10*, *PIGR*, *CD86*, *DUSP6*, *TLR3*, *STAT2*, *IL-6*, *IL-12*, *IL-1β*, *TNF-α*, *METTL3*, *METTL14*, *WTAP*, *FTO*, *ALKBH5*. *GAPDH* was used as the housekeeping gene. The primers used in this study are listed in Supplementary Table S1.

Western blotting analysis

Total proteins were extracted using a NE-PER kit (Nuclear and Cytoplasmic Extraction Reagents, Thermo Fisher Scientific) according to the manufacturer's protocol. BCA kit (Nanjing Keygen Biotech) was used to normalize protein levels. Proteins were transferred to PVDF membranes, which were then immunoblotted with relevant primary detection antibodies [METTL3 (1:1,000, EPR18810, Abcam, China), WTAP (1:1,000, EPR18744, Abcam, China), ALKBH5 (1:1,000, EPR18958, Abcam, China), GAPDH

(1:4,000)] followed by secondary detection antibody [horseradish peroxidase (HRP) conjugated goat anti-rabbit IgG (Abcam, UK, 1:5,000)].

Statistical analyses

The $2^{-\Delta\Delta Ct}$ method [25] was used to assess relative gene expression. SPSS 18.0 (SPSS, Inc., IL, USA) was used for statistical analyses. Data are expressed as mean ± standard deviation (SD) and were compared using Student's *t*-test. $P < 0.05$ indicated statistical significance.

Results

Effects of DON on IPEC-J2 cell viability, inflammation, apoptosis

In this study, DON treatment was associated with a marked reduction in the viability of IPEC-J2 cells (Fig. 1a). In comparison with the control group, cell viability significantly decreased upon DON treatment for 48 h ($P < 0.01$, Fig. 1a); moreover, cell confluency of the DON-treated group was lower than that of the control group, and cell morphology showed an obvious alteration (Fig. 1b). We also found that DON-treated cells exhibited significantly higher expression levels of *IL-6*, *IL-12*, *IL-1β*, and *TNF-α* relative to control cells ($P < 0.05$; Fig. 1c). Consistent with these findings, DON-treated cells showed significantly higher rates of apoptotic cell death relative to control cells, as assessed via flow cytometry ($P < 0.01$; Fig. 1d-e).

Transcriptome-wide assessment of DON-related m^{6}A methylation profiles

Transcriptome-wide m^{6}A-sequencing (m^{6}A-seq) and RNA-seq of DON-treated and control cells were performed. These two datasets yielded 33.62–43.03 million and 42.17–43.31 million clean reads, respectively, with the RNA-seq dataset also serving as the m^{6}A-seq input library in this study (Table S2). Of these clean reads, 80.22% and 85.58% mapped to the reference genome (Sscrofa11.1), respectively.

Model-based ChIP-seq (MACS) analyses led to the identification of 15,879 and 13,088 m^{6}A peaks in DON-treated and control samples, corresponding to the transcripts of 7265 and 6354 genes, respectively (Fig. 2a-b). Ben diagram analyses revealed that 10,473 m^{6}A peaks and 5649 m^{6}A-modified genes were detectable in both the groups. In comparison with the control group, the DON-treated group exhibited 2615 new peaks and 5406 peaks that were no longer detectable, confirming that there were substantial differences in global m^{6}A modification patterns between the groups (Fig. 2c). In addition, m^{6}A peaks were found to be characterized by the canonical GGACU motif in the groups (Fig. 2d).

We next sought to understand m^{6}A-modified peak distributions on a per-gene basis and determined that approximately 30% of all modified genes (2321/7970) exhibited a unique m^{6}A modification peak. Most modified genes (5077/7970) exhibited between one and three m^{6}A-modified sites (Fig. 2e), while genes unique to the DON-treated group typically exhibited only one m^{6}A-modified site relative to m^{6}A-modified genes that were unique to the control group (Fig. 2f).

In addition, for both the groups, we assessed m^{6}A peak distributions throughout the entire transcriptome to determine the presence of any treatment-specific sites of preferential modification. The m^{6}A peaks were thus separated into the start codon (startC), 5'-UTR, CDS, stopC, and 3'-UTR peaks based on their transcript locations. A Metagene profile of peak density revealed these m^{6}A modifications to be specifically enriched in startC and stopC regions (Fig. 2g). Total and unique m^{6}A peaks were particularly enriched in the vicinity of CDS and start/stopC regions (Fig. 2h–j).

Enrichment of m^{6}A-modified genes in signaling pathways

We next compared the differences in m^{6}A peak abundance between the DON-treated and control groups. Of the 10,473 m^{6}A peaks that were evident in both the groups, we selected 3871 differentially methylated sites for further analyses. Relative to the control group, 2156 significantly hypermethylated m^{6}A peaks (Table S3) and 1715 significantly hypomethylated m^{6}A peaks (Table S4) were detected in the DON-treated group (fold change ≥ 2 and $P < 0.05$; Fig. 3a). The Integrative Genomics Viewer tool was used to visualize these methylated sites, which revealed that the GGACU motif surrounded the corresponding m^{6}A peaks in the DON-treated and control groups (Fig. 3b).

To assess the potential biological impact of m^6A modifications on DON-treated cells, we performed GO and KEGG pathway enrichment analyses of differentially methylated genes. We found that the genes harboring hypermethylated m^6A sites in DON-treated samples were enriched in many signaling pathways, including the TNF, TGF-β, and NF-κB signaling pathways (Fig. 3c-d, Table S5-S6). Moreover, the transcripts with DON-specific m^6A peaks were found to be involved in several biological processes, including the TNF signaling pathway (Fig. 3e-f).

Identification of differentially expressed genes (DEGs) in DON-treated cells

The aforementioned m^6A-seq input library was utilized as an RNA-seq dataset for elucidating global mRNA expression patterns in DON-treated and control cells. Scatter plots were constructed and hierarchical clustering analyses were performed using these RNA-seq data (Fig. 4a-b). In total, 1776 DEGs were identified upon comparing DON-treated and control samples; 728 genes were upregulated (Table S7) and 1048 were downregulated (Table S8) (fold change > 2 and $P < 0.05$) in DON-treated samples. GO enrichment analyses indicated that upregulated genes in DON-treated cells were involved in processes such as gene expression and RNA metabolism (Fig. 4c), while KEGG pathway enrichment analyses revealed these genes to be significantly enriched in the TNF, NOD-like receptor, and MAPK signaling pathways (Fig. 4d-e, Table S9-S10).

Conjoint analysis of m^6A-RIP-seq and RNA-seq data

Conjoint analyses of our m^6A-RIP-seq and RNA-seq datasets revealed a strong positive correlation ($R = 0.93$, $P < 0.0001$) between differential m^6A methylation and mRNA expression (Fig. 5a). Of the 2156 hypermethylated m^6A sites detected via m^6A-seq, 364 genes were also upregulated (“hyper-up”) and 10 were downregulated (“hyper-down”) at the mRNA level. In contrast, only three genes exhibiting hypomethylated m^6A sites were upregulated (“hypo-up”), while 356 were downregulated (“hypo-down”) at the mRNA level (Fig. 5b). Notably, 364/367 (99%) upregulated mRNA transcripts in DON-treated samples were associated with hypermethylated m^6A peaks. In addition, substantially more “hyper-up” and “hypo-down” genes were detected relative to “hyper-down” and “hypo-up” genes (Fig. 5b). Together, these data suggested that m^6A hypermethylation is typically associated with the upregulation of gene expression in DON-treated cells.

We then selected 41 candidate genes associated with DON-related pathways (TNF, NF-κB, NOD-like receptor, and MAPK signaling pathways) that exhibited significant changes in both m^6A abundance and mRNA transcript expression in DON-treated cells relative to control cells (Table 1, Fig. 5c). Next, m^6A peak locations in RNA transcripts were assessed by analyzing the overall expression levels of m^6A-methylated and non-m^6A-methylated transcripts in DON-treated and control samples (Fig. 5d). We further analyzed the transcripts that had been classified into subgroups (startC, 5'-UTR, CDS, stopC, and 3'-UTR) based on their m^6A modification sites. All m^6A peaks were analyzed, as were those that were unique to DON-treated and control samples. We found that the transcripts with m^6A modifications proximal to CDS were typically expressed at significantly lower levels relative to those harboring stopC modifications ($P < 0.01$, Fig. 5e). Different genes exhibit variable numbers of m^6A-modified sites, as mentioned earlier. We found that a higher number of m^6A-modified sites per gene was associated with upregulated gene expression (Fig. 5f). While gene expression is controlled by many complex mechanisms, differential m^6A modifications seem to clearly impact gene expression; further studies are thus warranted.

Table 1

List of 41 genes that exhibited a significant change both at the m^{6}A level and in mRNA transcript abundance in DON-treated IPEC-J2 cells as compared with control cells

Gene	Pattern	Chr	m^{6}A level change					mRNA level change		
			Peak region	Peak start	Peak end	Fold change	p-value	Strand	Fold change	p-value
DUSP3	Hyper-up	chr12	stopC	19346441	19346980	2.7687	1.84E-11	+	2.4357	5.00E-05
TNFAIP3	Hyper-up	chr1	stopC	26477694	26478020	2.8919	3.82E-09	-	2.5494	5.00E-05
GADD45A	Hyper-up	chr6	startC	144940801	144941475	2.9203	1.24E-08	-	3.1914	5.00E-05
CSF2	Hyper-up	chr2	stopC	134356721	134357200	85.6210	3.87E-09	+	41.0167	0.00265
KITLG	Hyper-up	chr5	3'UTR	94105866	94106700	6.0816	1.49E-08	+	5.1153	5.00E-05
BIRC3	Hyper-up	chr9	startC	33044581	33045625	2.7765	2.27E-10	+	5.3239	5.00E-05
PDPK1	Hyper-up	chr3	stopC	39434321	39434920	2.3270	8.72E-11	-	2.3343	5.00E-05
CRK	Hyper-up	chr12	CDS	47657981	47658440	2.8193	2.40E-10	-	2.0419	5.00E-05
KLF6	Hyper-up	chr10	CDS	66491750	66492174	2.6507	4.47E-08	+	2.1633	5.00E-05
PPM1A	Hyper-up	chr1	5'UTR	189279752	189280610	2.5586	7.38E-09	+	2.1644	5.00E-05
GADD45B	Hyper-up	chr2	stopC	76107781	76108656	9.7123	1.07E-06	-	10.2064	5.00E-05
VCAM1	Hyper-up	chr4	CDS	117507887	117508199	20.0952	2.36E-12	-	9.9608	5.00E-05
DDIT3	Hyper-up	chr5	stopC	22785381	22786030	3.7200	2.98E-09	-	3.1181	0.0009
RAP1A	Hyper-up	chr4	startC	108676581	108677320	3.5678	2.95E-11	-	2.3491	5.00E-05
RELB	Hyper-up	chr6	CDS	51479541	51480160	2.8405	1.06E-10	+	2.5145	5.00E-05
KLF10	Hyper-up	chr4	startC	34429922	34430291	4.4327	1.82E-09	+	6.7444	5.00E-05
NFKBIE	Hyper-up	chr7	stopC	39255074	39255380	5.0043	1.59E-11	-	5.0155	5.00E-05
CCR7	Hyper-up	chr12	stopC	21868261	21869000	17.6960	4.03E-12	+	11.8906	5.00E-05
CLCF1	Hyper-up	chr2	stopC	5151801	5152580	5.7717	1.91E-11	+	4.1889	5.00E-05
DUSP10	Hyper-up	chr10	stopC	10867141	10867691	8.7014	2.65E-09	-	4.6017	5.00E-05
CCL5	Hyper-up	chr12	stopC	39658801	39659121	5.5442	1.10E-09	+	3.9232	5.00E-05

Gene	Pattern	Chr	m^{6}A level change					mRNA level change		
			Peak region	Peak start	Peak end	Fold change	p-value	Strand	Fold change	p-value
ICAM1	Hyper-up	chr2	stopC	69106756	69107600	2.9456	2.86E-09	+	2.0062	5.00E-05
PRKCA	Hyper-up	chr12	3'UTR	13262181	13263100	3.0166	5.13E-11	+	2.5048	5.00E-05
TGFB1	Hypo-down	chr6	3'UTR	49333561	49334280	11.6198	1.01E-08	-	-2.4351	5.00E-05
BCL3	Hypo-down	chr6	stopC	51265021	51265354	2.0353	2.17E-08	+	-2.0036	5.00E-05
TEC	Hypo-down	chr8	CDS	38051181	38051723	2.5395	1.38E-11	-	-4.3544	5.00E-05
STAT2	Hypo-down	chr5	stopC	21733029	21733480	5.1305	2.77E-09	-	-4.5569	5.00E-05
PIGR	Hypo-down	chr9	5'UTR	67553941	67554580	30.4601	1.66E-10	-	-23.3819	5.00E-05
RFX5	Hypo-down	chr4	stopC	97904201	97904663	2.0043	4.20E-09	+	-2.3931	5.00E-05
DAXX	Hypo-down	chr7	CDS	29680121	29680480	3.6822	4.98E-13	-	-2.2014	5.00E-05
DUSP6	Hypo-down	chr5	stopC	93307561	93308040	58.5000	2.30E-06	+	-3.3500	5.00E-05
TRIM25	Hypo-down	chr12	stopC	33187481	33187871	2.2950	1.12E-08	-	-3.2655	5.00E-05
PRLR	Hypo-down	chr16	stopC	20637556	20638360	6.0164	1.41E-10	-	-6.8650	0.0005
FOS	Hypo-down	chr7	stopC	98451361	98452400	7.4379	2.59E-09	+	-8.2442	5.00E-05
CD86	Hypo-down	chr13	3'UTR	138427841	138429760	2.5790	8.54E-12	-	-2.5451	5.00E-05
IFNAR1	Hypo-down	chr13	stopC	196949349	196950532	2.0459	3.90E-10	+	-2.3086	5.00E-05
IL4R	Hypo-down	chr3	stopC	19528281	19528874	2.4307	1.23E-09	-	-2.1698	5.00E-05
ELK4	Hypo-down	chr9	CDS	66315867	66316374	2.6963	1.43E-11	-	-2.3659	5.00E-05
DDX58	Hypo-down	chr10	CDS	33931532	33932040	52.9034	1.21E-08	+	-51.1088	5.00E-05
TNFRSF21	Hypo-down	chr7	CDS	42066848	42067440	2.9831	1.26E-09	-	-3.5779	5.00E-05
TLR3	Hypo-down	chr15	startC	46969005	46969457	2.1686	2.51E-10	+	-3.1485	5.00E-05

To comprehensively elucidate the mechanisms regulating DON-induced cellular damage, we constructed a protein–protein interaction (PPI) network of m^{6}A-modified genes using the STRING database. The resultant network contained 41 nodes and 152 relationship pairs (Supplementary Table S11), and it was visualized using Cytoscape [26]. CSF2 was the most central protein in

this network (Fig. 6), and *CSF2* was a DEM and DMG in RNA-seq and m^{6}A-seq analyses, respectively, exhibiting a significant difference in its expression level in DON-treated cells (Table 1). To further validate our sequencing results, we performed qPCR to assess the expression level of several hyper- and hypomethylated genes (*CSF2*, *KLF6*, *CCR7*, *CCL5*, *KLF10*, *PIGR*, *CD86*, *DUSP6*, *TLR3*, and *STAT2*), and we found the expression levels to be similar to those detected using RNA-seq (Fig. 7). Notably, the expression of *CSF2* was markedly upregulated in DON-treated cells ($P < 0.01$).

Expression change of m^{6}A methyl marks in DON-treated IPEC-J2 cells

To gain insights into how the m^{6}A methyl marks regulated the DON-induced damage, we analyzed the mRNA and protein expression profiles of three m^{6}A writers (METTL3, METTL14, and WTAP) and two m^{6}A erasers (ALKBH5 and FTO) in DON-treated IPEC-J2 cells. qPCR detection showed (Fig. 8a), the expression of ALKBH5 was significantly upregulated in DON-treated cells ($P < 0.05$), while the expression of METTL3 and WTAP were significantly downregulated in DON-treated cells ($P < 0.05$). Further validation of western blot showed, the protein expression of METTL3 was markedly downregulated in DON-treated cells, but the change of ALKBH5 and WTAP expression were not obvious.

Discussion

The m^{6}A modification is the most common internal epitranscriptomic marker within mammalian mRNAs. The MeRIP-seq approach has been widely used to characterize m^{6}A methylation profiles in a range of species. Dominissini et al. (2012) reported the successful construction of human and murine m^{6}A methylation profiles and investigated transcriptome-wide m^{6}A methylation patterns in these species [3]. Some other studies were able to characterize m^{6}A methylation profiles in *Arabidopsis thaliana* [27], *Oryza sativa* [28], and *Saccharomyces cerevisiae* [29]. However, only few studies have assessed porcine m^{6}A methylation profiles to date. In this study, we characterized transcriptome-wide m^{6}A modification patterns in IPEC-J2 cells using the MeRIP-seq approach. We found that the m^{6}A modification sites were primarily enriched in CDS and start/stopC regions, with relatively few sites in 3'-UTR and 5'-UTR, and this result was consistent with that of an earlier study involving porcine liver tissues [12]. Similarly, m^{6}A peaks have been reported to be primarily concentrated around TSS and stopC regions in human cells. In mice, these peaks were more abundant throughout the internal region of modified mRNAs, with the following distribution frequencies: 37% CDS, 30% stopC, 20% 3'-UTR, and 13% TSS [30]. Overall, these findings demonstrate that at a high level, m^{6}A modification profiles in mammalian transcriptomes are similar across species. In contrast, in case of *A. thaliana*, the m^{6}A modification sites were primarily enriched in 3'-UTR and stop/startC regions, and distinct motifs in m^{6}A-modified startC regions were noted in *A. thaliana* relative to those observed in mammals [27]. Further, in case of *O. sativa*, the majority of the m^{6}A modification sites were found to be distributed in intergenic regions, with 70% of such sites being found in CDS and 3'-UTR, and 20% in intronic regions and 5'-UTR [28]. These findings suggest that m^{6}A methylation patterns are species specific. In general, most m^{6}A methylation sites in mammals and plants were significantly enriched in stopC regions and 3'-UTR, suggesting that these modification patterns are consistent with the typical topological m^{6}A patterning of mature mRNAs [27, 28, 30]. The m^{6}A enrichment in these terminal regions seems to be associated with RNA stability and signal transduction, and may further regulate the recruitment of specific factors necessary for mRNA transport or translation (Wang et al., 2014; Li et al., 2014). The RRACH consensus sequence is characteristic of the canonical conserved domains at which m^{6}A methylation occurs [31–33], and this was confirmed via our m^{6}A high-throughput sequencing results [34–36]. No such RRACH sequence, however, was detected in *O. sativa* mRNAs [28]. Further studies should be conducted to explore differences in species-specific m^{6}A consensus sequences.

At a functional level, m^{6}A modifications modulate diverse processes, including metabolism, differentiation, and disease pathology [11, 37]. m^{6}A methylation patterns vary among tissues and in response to specific environmental stimuli. Dominissini et al. (2012) observed variances in these patterns in human hepatoma (HepG2) cells following treatment with a range of factors, including heat shock, interferons, and ultraviolet radiation [3]. Environment- and stimuli-specific m^{6}A methylation patterns have also been studied using murine embryonic stem cells, embryonic fibroblasts, and preadipocytes [38, 39]. In this study, on comparing differences in m^{6}A methylation patterns between DON-treated and control IPEC-J2 cells, genes that were both upregulated and more frequently m^{6}A modified were found to be associated with various immunological signaling pathways, such as the TNF and MAPK pathways. Wang et al. (2018) revealed that DON treatment induces toxicity and apoptotic cell death

in piglet hippocampal nerve cells via the MAPK signaling pathway [40]. Further, Zhang et al. (2020) reported that in IPEC-J2 cells, DON treatment induced the production of proinflammatory factors by activating p38 and ERK1/2 [18], while Wang et al. (2019) showed that treating IPEC-J2 cells with DON caused inflammatory injury via activation of the NF-κB signaling pathway [41]. With regard to the m^{6}A-modified genes identified in this study, our RNA-seq and qPCR analyses indicated that *CSF2* was differentially expressed the most significantly in DON-treated cells, and CSF2 was the most central protein in the constructed PPI network (Fig. 6). *CSF2* is involved in the TNF signaling pathway and thus regulates human disease pathology [42–44], which suggests that *CSF2* is of key functional relevance in the context of DON-induced toxicity. Few studies to date, however, have analyzed porcine *CSF2*, indicating that it is pivotal to systematically assess the association between *CSF2* expression and DON treatment via Cas9-mediated knockout and overexpression experiments.

Generally, m^{6}A modification is deposited to RNAs by the m^{6}A methyltransferase complex (METTL3, METTL14, WTAP) [45], and reversed by demethylases (FTO, ALKBH5) [46, 47]. Deoxynivalenol (DON), as mycotoxin, does not encode any known methyltransferase or demethylases, host methyltransferases and demethylases appear to play a critical role in m^{6}A methylation. To explore the role of m^{6}A methyltransferase and demethylases in DON-induced damage, we evaluated the expression patterns of METTL3, METTL14, WTAP, FTO and ALKBH5 in DON-treated IPEC-J2 cells. Among these, METTL3 showed the most obvious difference between normal cells and DON-treated cells. METTL3, as a key enzyme of m^{6}A methylation modification, can attenuate LPS induced inflammatory response in macrophages through NF-κB signaling pathway [48]. METTL3 knockdown inhibits osteoblast differentiation and activates the inflammatory response by regulating MAPK signaling in LPS-induced inflammation [49]. Moreover, the m^{6}A methylome analysis showed that the upregulated m^{6}A-modified genes in DON-treated IPEC-J2 cells mainly participate in the TNF and MAPK signaling pathways. Accordingly, the similar expression pattern of the m^{6}A methyltransferase METTL3 and m^{6}A-modified genes suggested that METTL3 might play a functional role in DON-induced inflammatory response, but further verification will be required in the future.

Conclusions

To summarize, this study characterized m^{6}A modification patterns in IPEC-J2 cells, and provide evidence that *CSF2* seems to play key roles in modulating inflammatory responses in the presence of DON. Further studies should be conducted by utilizing RNA methylases (METTL3) to comprehensively analyze the role of m^{6}A methylation in the regulation of responses of porcine cells to DON treatment.

Abbreviations

DON: Deoxynivalenol; m^{6}A: N^6-Methyladenosine; IPEC-J2: intestinal porcine epithelial cells; TNF: tumor necrosis factor; TSS: transcriptional start site; CDS: coding sequence; UTR: untranslated region; MeRIP-seq: methylated RNA immunoprecipitation sequencing; GO: gene ontology; KEGG: Kyoto Encyclopedia of Genes and Genomes; DEGs: differentially expressed genes

Declarations

Ethics approval and consent to participate

The Institutional Animal Care and Use Committee (IACUC) of the Yangzhou University Animal Experiments Ethics Committee approved the animal study proposal, with the permit number: SYXK(Su) IACUC 2012-0029.

Acknowledgements

We thank CloudSeq Biotech Inc. (Shanghai, China) for performing high-throughput sequencing and for their bioinformatics support.

Funding

This study was supported by grants from the Natural Science Foundation of Jiangsu Province, China (BK20180899), the National Natural Science Funds (31972535, 31772560), the Natural Science Foundation of Yangzhou City, China (YZ2018102), the Qingnan Project of Yangzhou University, the Earmarked Fund for Jiangsu Agricultural Industry Technology System, and the Priority Academic Program Development of Jiangsu Higher Education Institutions.

Authors' contributions

WBB conceived and designed the experiments. ZCW, CX and FHW performed the experiments, including cell treatment, qPCR assay, and wrote the manuscript. ZCW performed the statistical analyses. SG and SLW helped to revise the manuscript. All authors read and approved the final version of this manuscript.

Availability of data and materials

The raw high-throughput m^{6}A and RNA-seq data have been uploaded to the Gene Expression Omnibus (GEO) database (GEO accession No.: GSE156078). The other datasets analysed in the current study are available from the corresponding author upon reasonable request.

Consent for publication

Not applicable.

Competing interests

All authors declare that they have no competing interests.

References

1. Li X, Xiong X, Yi C. Epitranscriptome sequencing technologies: decoding RNA modifications. Nat Methods. 2016;14(1):23–31.
2. Lence T, Paolantoni C, Worpenberg L, Roignant JY. Mechanistic insights into m^{6}A RNA enzymes. Biochimica et biophysica acta. Biochim Biophys Acta Gene Regul Mech. 2019;1862(3):222–9.
3. Dominissini D, Moshitch-Moshkovitz S, Schwartz S, Salmon-Divon M, Ungar L, Osenberg S, et al. Topology of the human and mouse m^{6}A RNA methylomes revealed by m^{6}A-seq. Nature. 2012;485(7397):201–6.
4. Zheng G, Dahl JA, Niu Y, Fedorcsak P, Huang CM, Li CJ, et al. ALKBH5 is a mammalian RNA demethylase that impacts RNA metabolism and mouse fertility. Mol Cell. 2013;49:18–
5. Yang Y, Hsu PJ, Chen YS, Yang YG. Dynamic transcriptomic m^{6}A decoration: writers, erasers, readers and functions in RNA metabolism. Cell Res, 2018;28(6):616–
6. Hao HJ, Hao SJ, Chen HH, Chen Z, Zhang YF, Wang J, et al. N6-methyladenosine modification and METTL3 modulate enterovirus 71 replication. Nucleic Acids Res. 2019;47(1):362–
7. Durbin AF, Wang C, Marcotrigiano J, et al. RNAs containing modified nucleotides fail to trigger RIG-I conformational changes for innate immune signaling. Mbio. 2016;7(5):e00833–
8. Karikó K, Buckstein M, NiH, Weissman D. Suppression of RNA recognition by Toll-like receptors: the impact of nucleoside modification and the evolutionary origin of RNA. Immunity. 2005;23(2):165–
9. Heng J, Tian M, Zhang W, Chen F, Guan W, Zhang S. Maternal heat stress regulates the early fat deposition partly through modification of m6A RNA methylation in neonatal piglets. Cell Stress Chaperones. 2019;24(3):635–
10. Lu NA, Li XM, Yu JY, Li Y. Curcumin Attenuates Lipopolysaccharide-Induced Hepatic Lipid Metabolism Disorder by Modification of m6A RNA Methylation in Piglets. Lipids. 2018;53(1):53–
11. Wu RF, Liu YH, Zhao YL, Bi Z, Yao YX, Liu Q, et al. m^{6}A methylation controls pluripotency of porcine induced pluripotent stem cells by targeting SOCS3/JAK2/STAT3 pathway in a YTHDF1/YTHDF2-orchestrated manner. Cell Death Dis. 2019;10(3):171.

12. He S, Wang H, Liu R, He MN, Che TD, Jin L, et al. mRNA N6-methyladenosine methylation of postnatal liver development in pig. PLoS One. 2017;12(3):e0173421.
13. Reddy KRN, Salleh B, Saad B, Abbas HK, Abel CA, Shier WT. An overview of mycotoxin contamination in foods and its implications for human health. Toxin Rev. 2010;29:3–
14. Pestka JJ. Deoxynivalenol: mechanisms of action, human exposure, and toxicological relevance. Arch Toxicol. 2010;84(9):663–679.
15. Diesing AK, Nossol C, Ponsuksili S, Wimmers K, Kluess J, Walk, et al. Gene regulation of intestinal porcine epithelial cells IPEC-J2 is dependent on the site of deoxynivalenol toxicological action. PLoS One. 2012;7:e34136.
16. Wang, S.; Yang, J.; Zhang, B, et al. Deoxynivalenol impairs porcine intestinal host defense peptide expression in weaned piglets and IPEC-J2 cells. Toxins 2018, 10, No. e541.
17. Ji X, Zheng W, Yao W. Protective Role of Hydrogen Gas on Oxidative Damage and Apoptosis in Intestinal Porcine Epithelial Cells (IPEC-J2) Induced by Deoxynivalenol: A Preliminary Study. Toxins (Basel). 2019;12(1):5.
18. Zhang H, Deng X, Zhou C, Wu W, Zhang H. Deoxynivalenol Induces Inflammation in IPEC-J2 Cells by Activating P38 Mapk And Erk1/2. Toxins (Basel). 2020;12(3):180.
19. Dominissini D, Moshitch-Moshkovitz S, Salmon-Divon M, Amariglio N, Rechavi G. Transcriptome-wide mapping of N6-methyladenosine by m6A-seq based on immunocapturing and massively parallel sequencing. Nat Protoc. 2013;8(1):176–
20. Martin M. Cutadapt removes adapter sequences from high-throughput sequencing reads. EMBnet J. 2011;17(1):10–
21. Kim D, Langmead B, Salzberg SL. HISAT: a fast spliced aligner with low memory requirements. Nat Methods. 2015;12(4):357–
22. Zhang Y, Liu T, Meyer CA, Eeckhoute J, Johnson DS , Bernstein BE, et al. Model-based Analysis of ChIP-Seq (MACS). Genome Biol. 2008;9:R137
23. Shen L, Shao NY, Liu X, Maze I, Feng J, Nestler EJ. diffReps: detecting differential chromatin modification sites from ChIP-seq data with biological replicates. PLoS O 2013;8(6):e65598.
24. Thorvaldsdottir H, Robinson JT, Mesirov JP. Integrative Genomics Viewer (IGV): high-performance genomics data visualization and exploration. Brief Bioinform. 2013;14:178–
25. Livak KJ, Schmittgen TD. Analysis of relative gene expression data using real-time quantitative PCR and $2^{-\Delta\Delta CT}$ Methods. 2001;25:402–8.
26. Shannon P, Markiel A, Ozier O, Baliga NS, Wang JT, Ramage D, et al. Cytoscape: a software environment for integrated models of biomolecular interaction networks. Genome Res. 2003;13(11):2498–
27. Luo GZ, MacQueen A, Zheng GQ, Duan HC, Dore LC, Lu Z, et al. Unique features of the m^6A methylome in *Arabidopsis thaliana*.Nat Commun. 2014;5:5630.
28. Li Y, Wang X, Li C, Hu S, Yu J, Song S. Transcriptome-wide N6-methyladenosine profiling of rice callus and leaf reveals the presence of tissue-specific competitors involved in selective mRNA modification. RNA Biol. 2014;11(9):1180–
29. Schwartz S, Agarwala SD, Mumbach MR, Jovanovic M, Mertins P, Shishkin A, et al. High-resolution mapping reveals a conserved, widespread, dynamic mRNA methylation program in yeast meiosis. Cell. 2013;155(6):1409–
30. Meyer KD, Saletore Y, Zumbo P, Elemento O, Mason CE, Jaffrey SR. Comprehensive analysis of mRNA methylation reveals enrichment in 3'UTRs and near stop codons. Cell. 2012;149(7):1635–
31. Harper JE, Miceli SM, Roberts RJ, Manley JL. Sequence specificity of the human mRNA N6-adenosine methylase in vitro. Nucleic Acids Res. 1990;18(19):5735–
32. Wei CM, Moss B. Nucleotide sequences at the N6-methyladenosine sites of HeLa cell messenger ribonucleic acid. Biochemistry. 1977;16(8):1672–
33. Csepany T, Lin A, Baldick CJ, Beemon K. Sequence specificity of mRNA N6-adenosine methyltransferase. J Biol Chem. 1990;265(33):20117–
34. Sai LL, Li Y, Zhang YC, Zhang J, Qu BP, Guo QM, et al. Distinct m^6A methylome profiles in poly(A) RNA from Xenopus laevis testis and that treated with atrazine. Chemosphere. 2020;245:125631.

35. Wang YJ, Zeng L, Liang C, Zan R, Ji WP, Zhang ZC, et al. Integrated analysis of transcriptome-wide m^6A methylome of osteosarcoma stem cells enriched by chemotherapy. Epigenomics. 2019;11(15):1693–
36. Wang Y, Mao J, Wang X, Lin Y, Hou GQ, Zhu J, et al. Genome-wide screening of altered m6A-tagged transcript profiles in the hippocampus after traumatic brain injury in mice. Epigenomics. 2019;11(7):805–
37. Lin S, Choe J, Du P, Triboulet R, Gregory RI. The m6A methyltransferase METTL3 promotes translation in human cancer cells. Mol Cell. 2016;62:335–
38. Zhao X, Yang Y, Sun BF, Shi Y, Yang X, Xiao W, et al. FTO-dependent demethylation of N6-methyladenosine regulates mRNA splicing and is required for adipogenesis. Cell Res. 2014;24(12):1403–
39. Geula S, Moshitch-Moshkovitz S, Dominissini D, Mansour AA, Kol N, Salmon-Divon M, et al. Stem cells. m6A mRNA methylation facilitates resolution of naïve pluripotency toward differentiation. Science. 2015;347(6225):1002–
40. Wang XC, Fan MX, Chu XY, Zhang YF, Rahman SU, Jiang YJ, et al. Deoxynivalenol induces toxicity and apoptosis in piglet hippocampal nerve cells via the MAPK signaling pathway. Toxicon. 2018;155:1–
41. Wang X, Zhang Y, Zhao J, Cao L, Zhu L, Huang YY, et al. Deoxynivalenol Induces Inflammatory Injury in IPEC-J2 Cells via NF-κB Signaling Pathway. Toxins (Basel). 2019;11(12):733.
42. Xu ZB, Zhang YY, Xu MF, Zheng X, Lin MX, Pan J, et al. Demethylation and Overexpression of CSF2 are Involved in Immune Response, Chemotherapy Resistance, and Poor Prognosis in Colorectal Cancer. Onco Targets Ther. 2019;12:11255–
43. Lee YY, Wu WJ, Huang CN, Li CC, Li WM, Yeh BW, et al. CSF2 overexpression is associated with STAT5 phosphorylation and poor prognosis in patients with urothelial carcinoma. J Cancer. 2016;7(6):711–
44. Chen WC, Wei JCC, Lu HF, Wong HSC, Woon PY, Hsu YW, et al. rs657075 (CSF2) is associated with the disease phenotype (BAS-G) of ankylosing spondylitis. Int J Mol Sci. 2017;18(1):83.
45. Scholler E, Weichmann F, Treiber T, Ringle S, Treiber N, Flatley A, et al. Interactions, localization, and phosphorylation of the m(6)A generating METTL3-METTL14-WTAP complex. RNA. 2018;24:499–
46. Jia G, Fu Y, Zhao X, Dai Q, Zheng G, Yang Y, et al. N6-Methyladenosine in nuclear RNA is a major substrate of the obesity-associated FTO. Nat Chem Biol. 2011;7:885–
47. Zheng G, Dahl JA, Niu Y, Fedorcsak P, Huang C, Li CJ, et al. ALKBH5 is a mammalian RNA demethylase that impacts RNA metabolism and mouse fertility. Mol Cell. 2013;49:18–
48. Wang J, Yan S, Lu H, Wang S, Xu D. METTL3 Attenuates LPS-Induced Inflammatory Response in Macrophages via NF-κB Signaling Pathway. Mediators Inflamm. 2019;2019:3120391.
49. Zhang Y, Gu X, Li D, Cai L, Xu Q. METTL3 Regulates Osteoblast Differentiation and Inflammatory Response via Smad Signaling and MAPK Signaling. Int J Mol Sci. 2019;21(1):199.

Figures

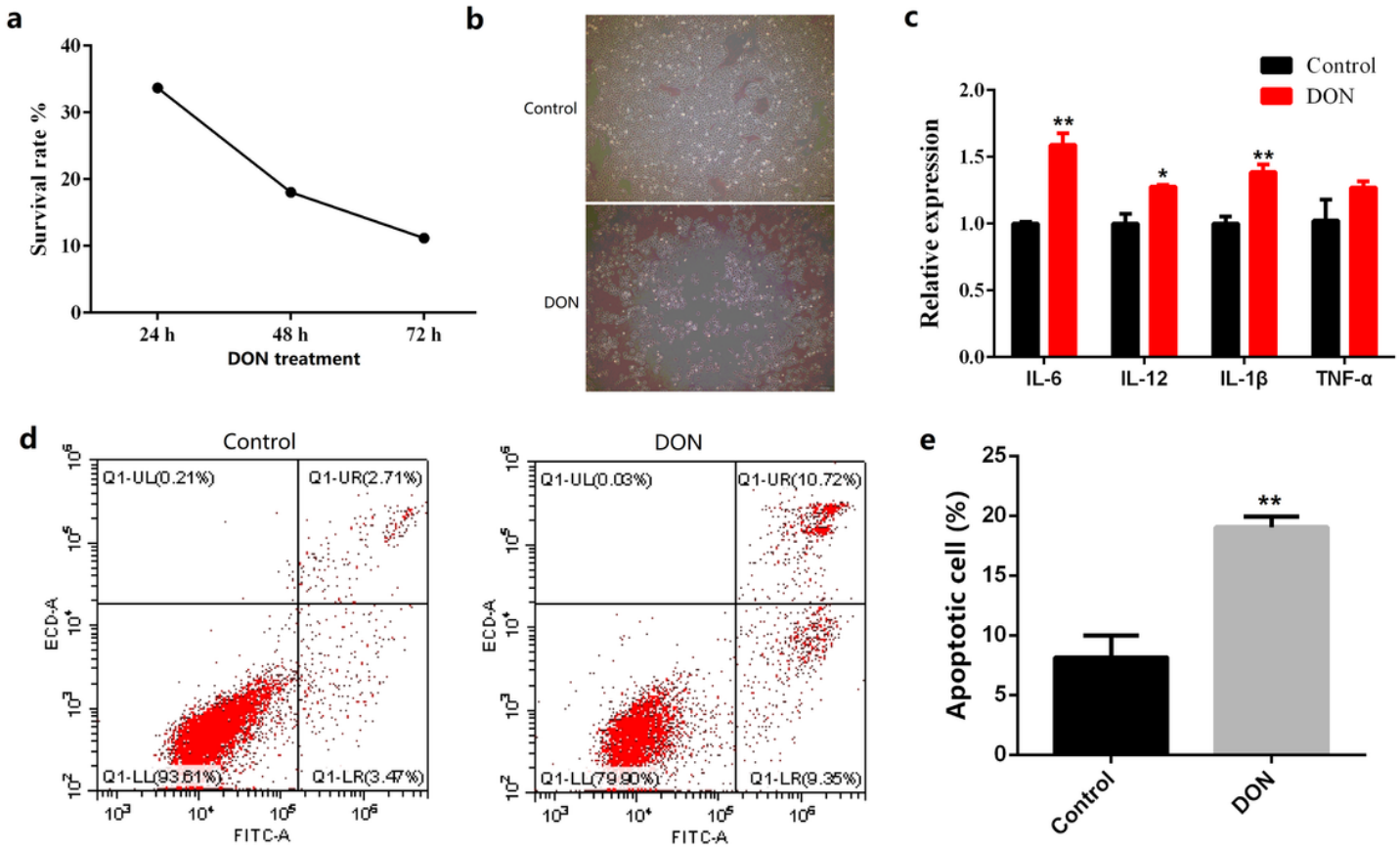

Figure 1

Effects of DON on IPEC-J2 cell viability, inflammation, and apoptosis. (a) IPEC-J2 cells were treated with DON for 24, 48, or 72 h, and the effect of DON on cell viability was assessed using the Cell Counting Kit-8 assay. (b) Morphology of IPEC-J2 cells. The control group was treated with an equal volume of solvent; the DON-treated group was treated with 1000 ng/mL DON. (c) Detection of inflammation-associated gene expression in DON-treated cells for 48 h. (d-e) Apoptotic cell death was assessed in DON-treated cells for 48 h. The rate of apoptosis was analyzed using flow cytometry. Data are expressed as mean ± SD from triplicate experiments. *P < 0.05, **P < 0.01.

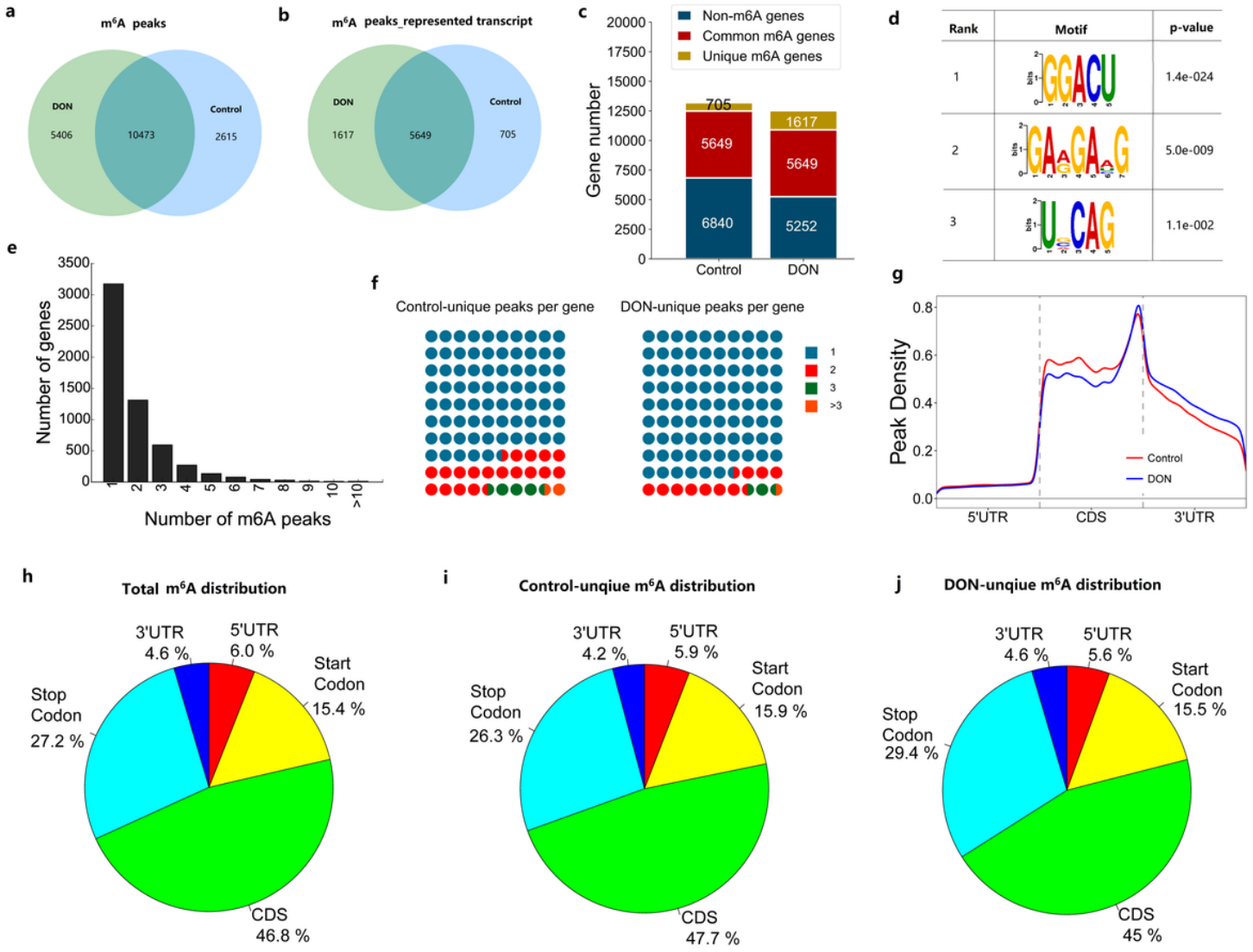

Figure 2

m6A-RIP-seq-mediated assessment of the m6A methylome of DON-treated IPEC-J2 cells. (a) Numbers of group-specific and common m6A peaks. (b) A Venn diagram was constructed to highlight m6A peaks present in DON-treated and control samples. (c) m6A-modified genes identified via m6A-seq. (d) A sequence diagram highlighting the conserved RRACH motif in m6A-containing peak regions. (e) Numbers of m6A-modified peaks per gene. (f) m6A-modified peak distributions on a per-gene basis in genes that were uniquely modified in DON-treated and control samples. (g) m6A peak density along a metagene. (h–j) Pie charts highlighting m6A peak distribution in different gene regions in DON-treated and control samples. DON, DON-treated IPEC-J2 cells; Control, untreated IPEC-J2 cells.

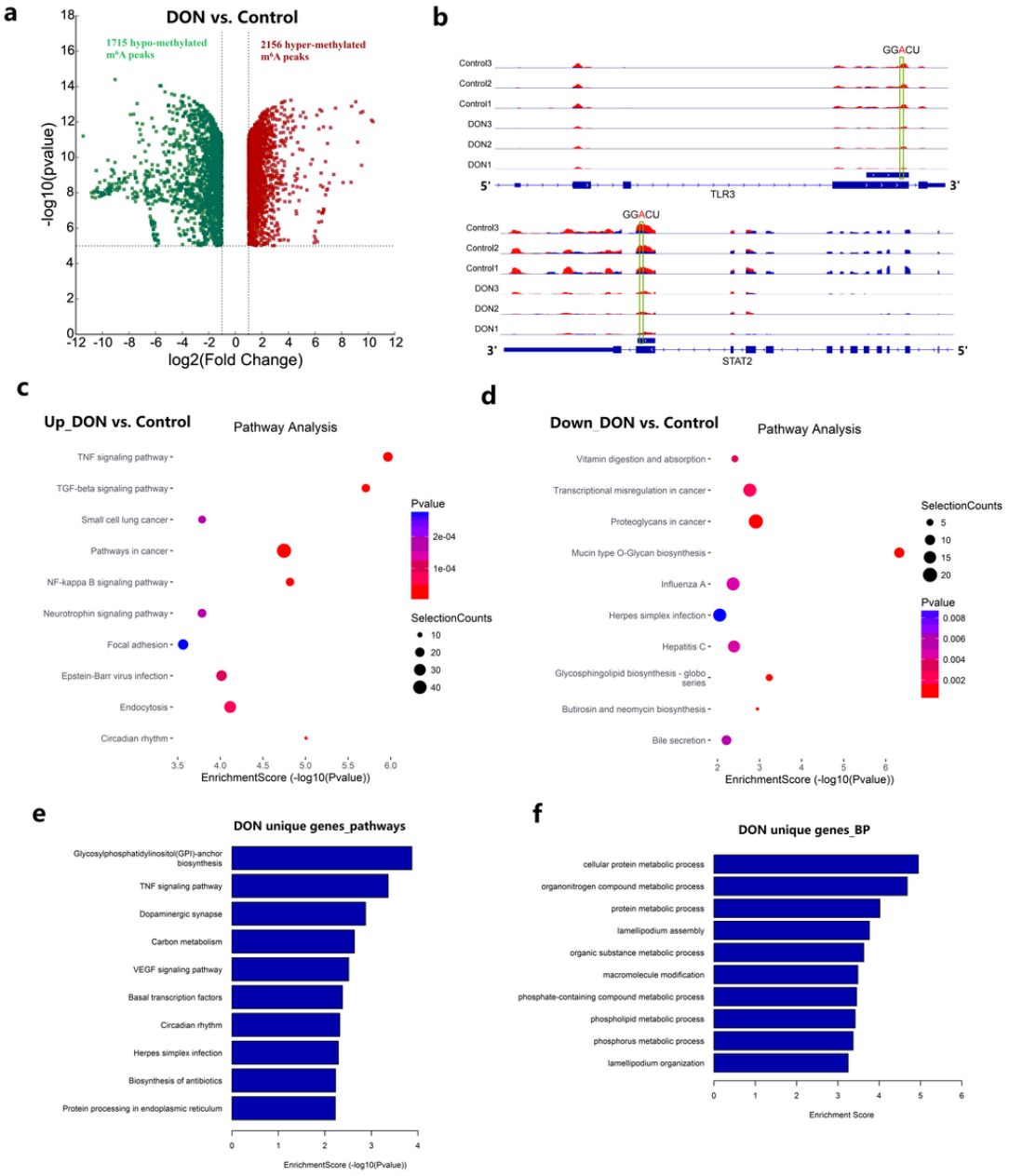

Figure 3

Global changes in m6A modification patterns in DON-treated IPEC-J2 cells relative to control cells. (a) Volcano plots highlighting distinct m6A peaks (fold change ≥ 2 and P < 0.05). (b) Visualization of TLR3 and STAT2 mRNA m6A modifications in DON-treated and control samples. (c-d) Pathway analyses of transcripts with significantly up- or downregulated m6A modification rates in DON-treated samples relative to control samples. (e) KEGG pathway analysis of transcripts with DON-specific m6A peaks. (f) GO analysis of biological processes associated with transcripts exhibiting DON-specific m6A peaks.

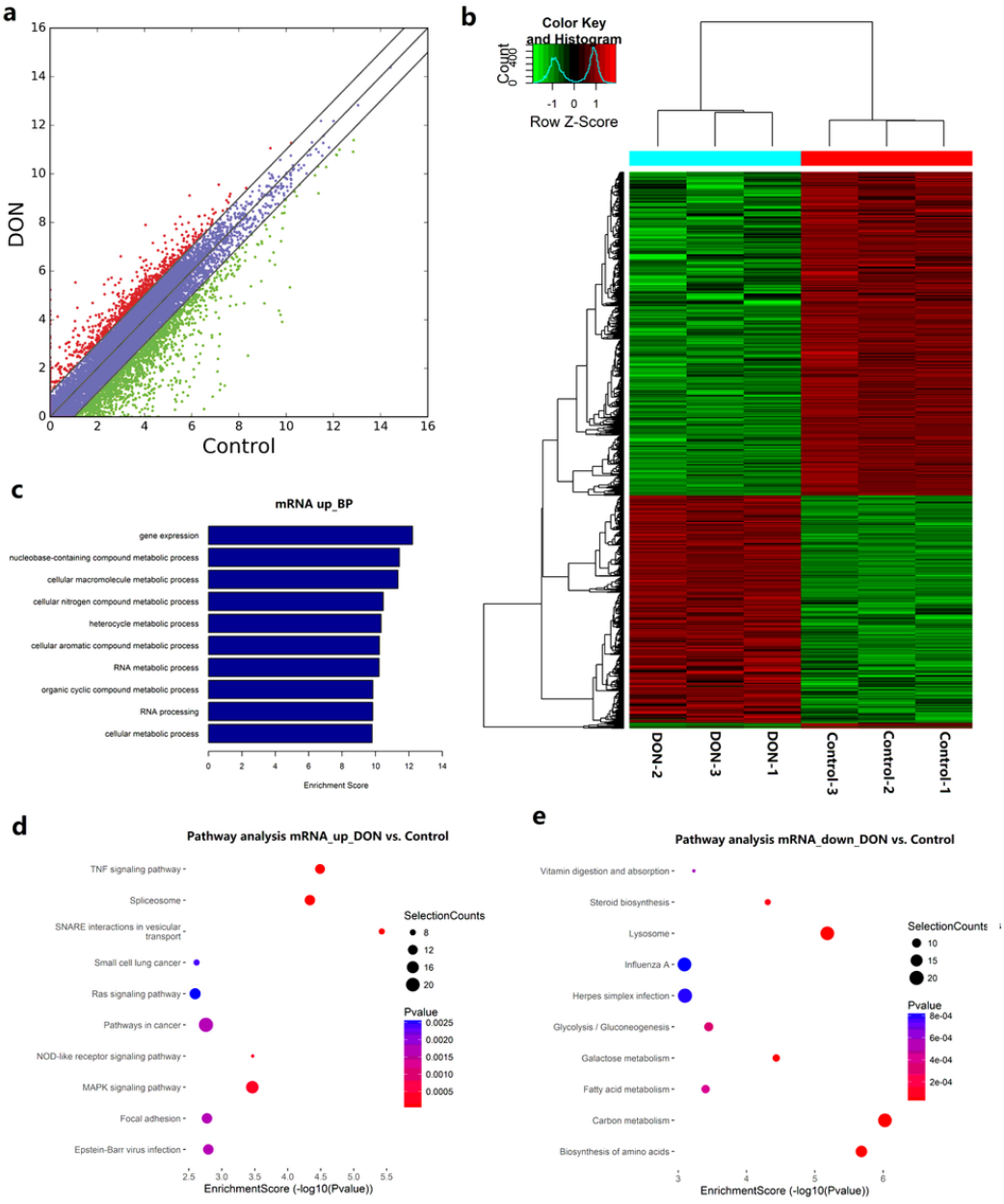

Figure 4

Identification of DEGs between DON-treated and control IPEC-J2 cells via RNA-seq. (a) Scatter plots showing DEGs in DON-treated and control cells (fold change ≥ 2 and P < 0.05). (b) Hierarchical clustering analysis of RNA-seq data from DON-treated and control cells. (c) GO analysis of biological processes enriched for genes upregulated in DON-treated samples. (d-e) KEGG pathway analysis of genes that were up- and downregulated in DON-treated samples relative to control samples.

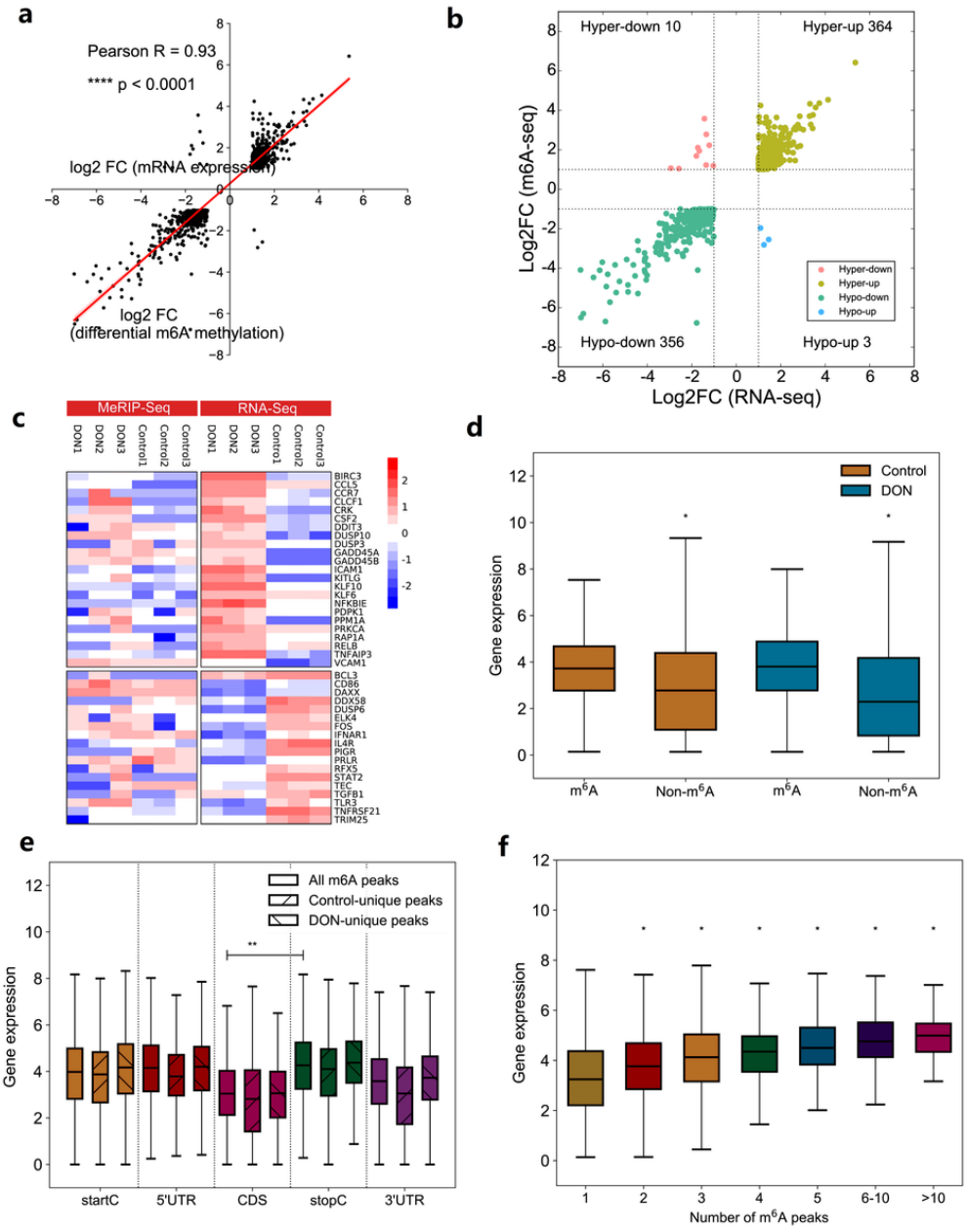

Figure 5

Conjoint analysis of m6A-RIP-seq and RNA-seq data. (a) Dot plots showing a positive correlation between overall m6A methylation and mRNA expression levels. (b) A four-quadrant graph highlighting DEGs containing differentially methylated m6A peaks. (c) Hierarchical clustering analysis of DEGs containing differentially methylated m6A peaks. (d) Overall expression levels of m6A-methylated and non-m6A-methylated transcripts in different groups. (e) m6A peak locations in RNA transcripts and relative gene expression levels in all m6A peaks, as well as in peaks unique to control and DON-treated cells. **P < 0.01 compared with the “stop codon” region. (f) Relative mRNA expression levels for transcripts containing different numbers of m6A peaks. *P < 0.05 relative to the first column (m6A peak = 1).

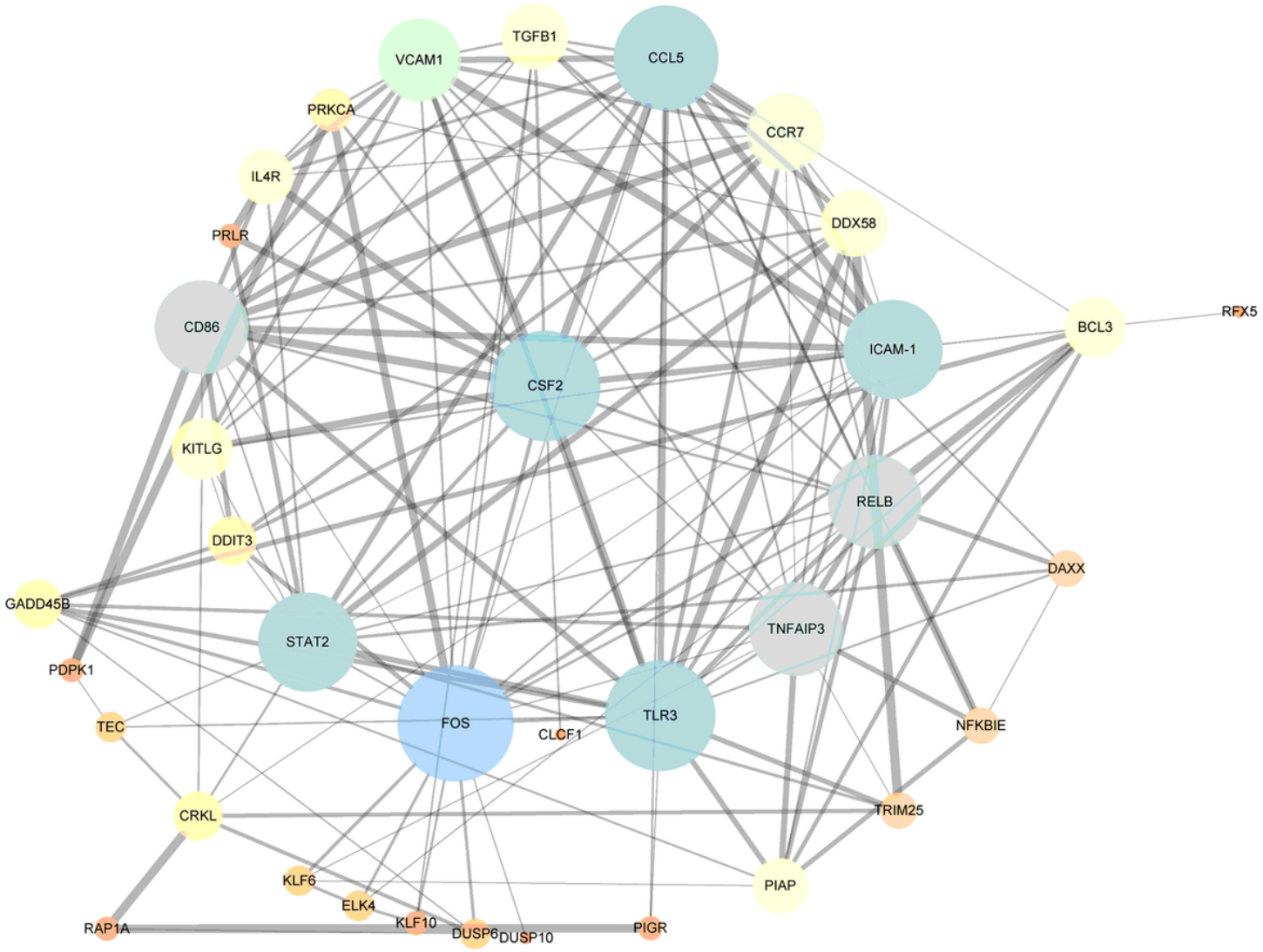

Figure 6

PPI network constructed with dysregulated m6A-modified genes. Cytoscape was used to visualize a network incorporating m6A-modified genes/proteins based on the conjoint analysis of m6A-RIP-seq and RNA-seq data.

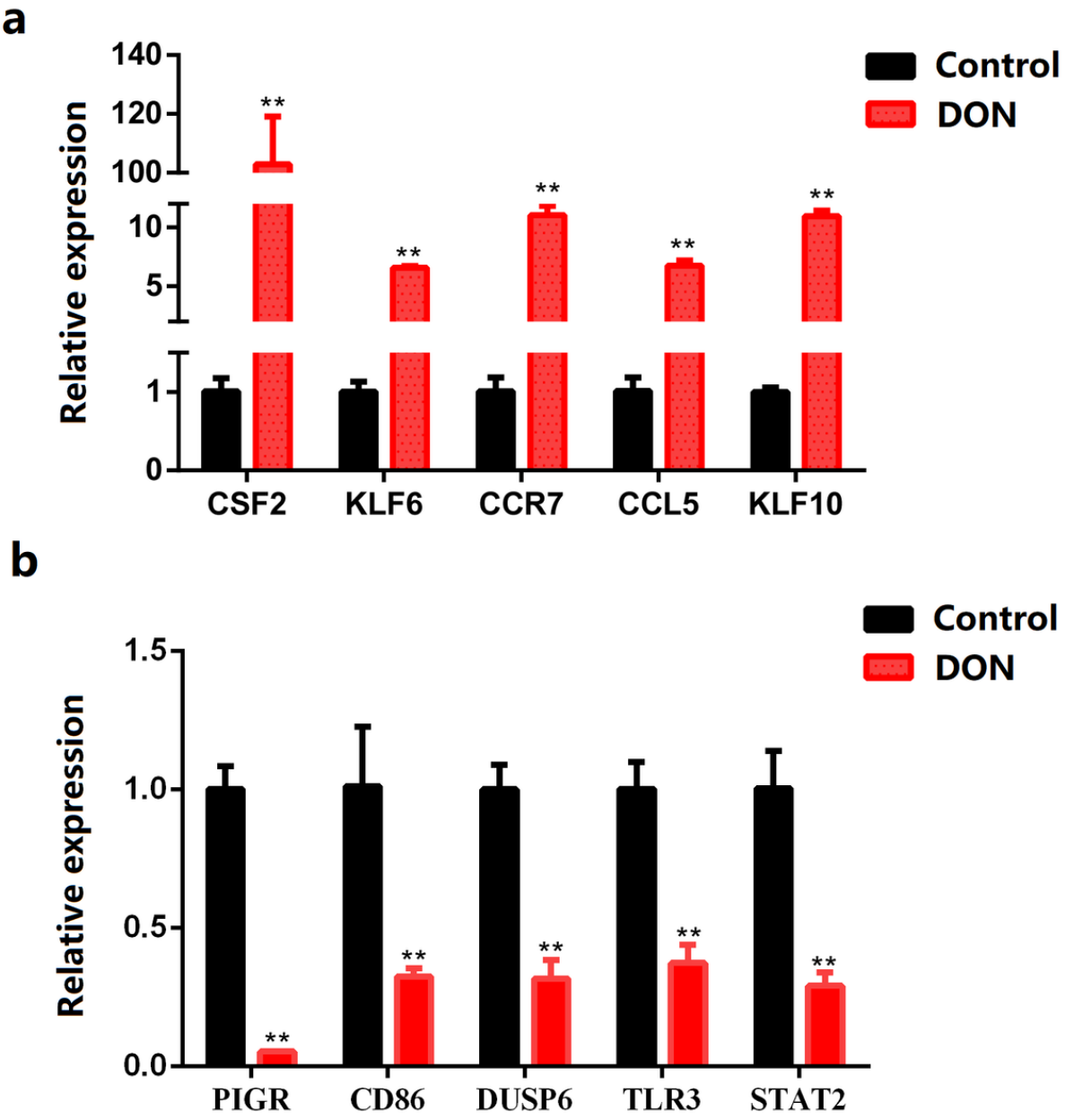

Figure 7

qPCR validation of dysregulated m6A-modified genes. Relative mRNA expression levels of 10 representative genes were assessed using qPCR. Bars correspond to mean values of four technical replicates. **P < 0.01.

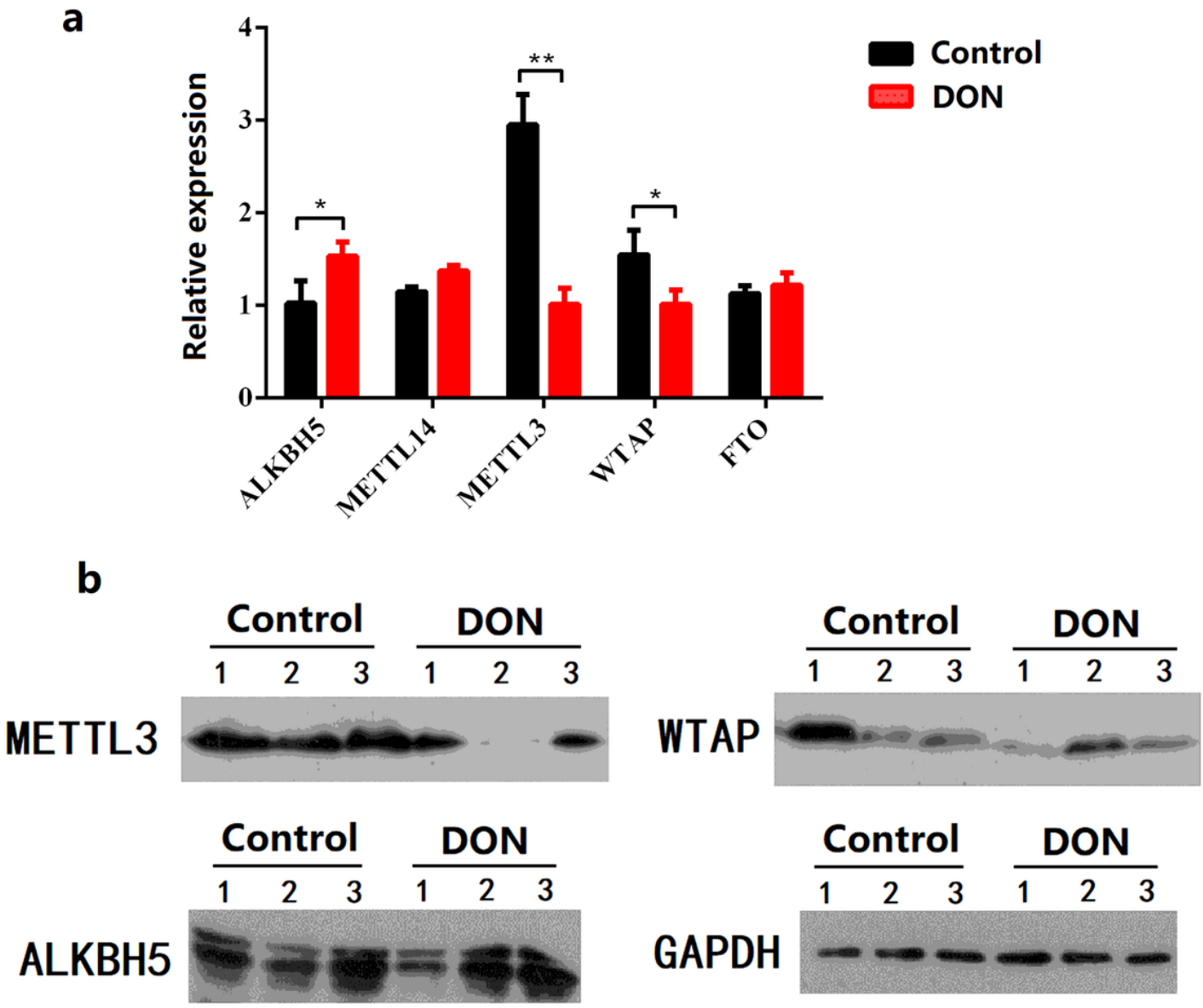

Figure 8

Expression detection of RNA methyltransferases and demethylases. (a) mRNA expression levels of RNA methyltransferases (METTL3, METTL14, WTAP) and demethylases (ALKBH5, FTO) were detected by qPCR. (b) western blot assay. *P < 0.05, **P < 0.01.

Supplementary Files

This is a list of supplementary files associated with this preprint. Click to download.

- SupplementaryTables.xlsx